Dalton Transactions

ROYAL SOCIETY OF CHEMISTRY

PAPER

View Article Online
View Journal | View Issue

Cite this: *Dalton Trans.*, 2026, **55**, 2046

Dual reaction pathway catalysis: base free transfer hydrogenation of aromatic aldehydes by a NiAl LDH catalyst *via in situ* Ni(0) formation

Anitya Sharma,[a] Sahil Kumar,†[a] Devendra Sharma, †[a] Ashish Bahuguna [b] and Venkata Krishnan *[a]

Formulating environmentally friendly and sustainable protocols for catalytic transfer hydrogenation (CTH) utilizing non-noble metal catalysts presents a considerable difficulty owing to their diminished activity relative to noble metals. This study presents a highly effective NiAl layered double hydroxide (LDH) catalyst produced by a traditional co-precipitation technique and activated *in situ* by isopropanol (IPA), functioning as both a hydrogen donor and a reducing agent. The CTH of benzaldehyde to benzyl alcohol proceeds efficiently under base-free conditions. Notably, during the reaction, a unique *in situ* transformation of Ni^{2+} species in the LDH to metallic Ni^{0} particles was observed, fundamentally shifting the reaction mechanism. Initial cycles proceed *via* a Meerwein–Ponndorf–Verley (MPV) pathway mediated by Lewis acidic and basic sites of the LDH. However, upon repeated use, the formation of Ni^{0} introduces a new metal-hydride-based pathway, wherein IPA dehydrogenation and aldehyde hydrogenation are facilitated by metallic Ni^{0} and Lewis acidic sites. This dual mechanistic pathway results in the dynamic evolution of the catalyst during the reaction. Control and poisoning studies further confirm the pivotal role of basic sites in the initial CTH process. This protocol provides an environmentally friendly and chemoselective method for synthesizing aromatic alcohols, demonstrating exceptional substrate tolerance and advantageous environmental metrics.

Received 23rd September 2025,
Accepted 19th December 2025

DOI: 10.1039/d5dt02279g

rsc.li/dalton

1. Introduction

Benzyl alcohol is a significant industrial chemical utilized as a solvent for inks, paints, lacquers, topical analgesics, oral healthcare medications, preservatives, and agents that reduce viscosity.[1,2] Despite its high demand in the industry, safer production of benzyl alcohol is still a challenge. Traditionally, carbonated sodium or potassium salts are employed in the production of benzyl alcohol from benzyl chloride. However, this process leads to the release of excess chlorine, which is highly toxic in nature and leads to the deterioration of the environment.[3] Another method for the production of benzyl alcohol is the catalytic oxidation of toluene.[4] Oxidation of toluene occurs at relatively higher temperatures and pressure. This leads to thermal degradation of catalysts and increases energy consumption and costs.[4] Partial oxidation leads to the formation of polyaromatics that deposit on the catalyst surface, blocking the active sites. The catalytic systems employ (Co–Mn–Br) as a catalyst. The halide leaching from the catalyst causes severe corrosion of the reactor and leads to waste disposal problems. Furthermore, the oxidation proceeds *via* three pathways: (i) side-chain reaction (desired), (ii) ring oxidation (undesired), and (iii) cracking reactions (undesired). This makes the process non-selective for benzyl alcohol formation. Alongside this, over-oxidation of benzyl alcohol leads to by-products such as benzaldehyde, benzoic acid and even CO_2 and H_2O in some cases.[5] This decreases the overall yield of the desired product. The hydrogenation of benzaldehyde has recently emerged as a favoured method for synthesizing benzyl alcohol. This can be achieved either by direct hydrogenation using molecular hydrogen or by the catalytic transfer hydrogenation (CTH) process using suitable hydrogen sources.[6]

Conventional hydrogenation using molecular hydrogen suffers from many drawbacks: (i) highly inflammable molecular hydrogen raises the risk of serious hazards, (ii) the handling of high-pressure hydrogen requires heavy and costly equipment raising the overall costs of the process. To overcome these problems, CTH uses a hydrogen source, such as formic acid, alcohols, water, *etc.*, as a safe and green alternative for the production of benzyl alcohol.[6–9] The advantages of CTH are the use of high-pressure reactors and elimination of

[a]*School of Chemical Sciences and Advanced Materials Research Center, Indian Institute of Technology Mandi, Kamand, Mandi 175075, Himachal Pradesh, India*
[b]*Dr Ambedkar Centre of Excellence, Hemvati Nandan Bahuguna Garhwal University (A Central University), Srinagar Garhwal, 246174 Uttarakhand, India.*
E-mail: vkn@iitmandi.ac.in
†These authors contributed equally to this work.

highly inflammable hydrogen gas; the hydrogen donors utilized in this process are cheap, readily available and act as solvents as well, enabling the reaction to be carried out under external solvent-free conditions. These salient features make CTH an attractive, green, and industrially relevant process.[6]

In recent decades, various homogeneous and heterogeneous catalysts have been explored for CTH. Traditional homogeneous catalysts consist of heavy metals, such as Ru, Rh, Ir, *etc.*, which have relatively low abundance, are highly expensive, and exhibit cellular toxicity.[10,11] In contrast, cost effective and non-noble metal-based catalysts are being employed to carry out the transfer hydrogenation process.[12–15] Although homogeneous catalysts are found to exhibit high catalytic activity, they tend to suffer from the following drawbacks such as the difficulty in separating the homogeneous catalysts from the reaction media and the catalysts being unstable at high temperatures and pressures. In contrast, heterogeneous catalysts have been extensively used for the CTH process. The heterogeneous catalysts exhibit advantages, such as scalable synthesis, easy separation of catalysts and high catalytic stability.[16–19] However, most of the heterogeneous catalytic systems cannot be employed on a large scale because they suffer from the following: (i) use of noble metals, which increases the overall cost of production of the catalyst, (ii) leaching of the catalyst from the support in the case of composites, or (iii) high pressure and temperature conditions employed for the synthesis of catalysts.[9,20] These disadvantages restrict the use of heterogeneous catalysts for carrying out hydrogenation reactions on a large scale.

In order to overcome these problems, layered double hydroxides (LDHs) have been employed for carrying out the transfer hydrogenation of aromatic aldehydes to the corresponding alcohols.[7,21] LDH is a class of synthetic anionic clays that consist of brucite-like layers with certain anions and water molecules in the interlayer space.[22] The brucite layer of LDH consists of M^{2+} and M^{3+} ions. LDH is a versatile material and exhibits properties like high surface area, tunable basicity, exchangeable cations in the brucite layer, and anions in interlayer space of the material, respectively.[15] These properties make the layered double hydroxides a suitable material for carrying out the CTH process.

In this work, we have synthesized a highly efficient and versatile non-noble metal-based nickel–aluminum layered double hydroxide (NiAl LDH) catalyst *via* a facile and scalable co-precipitation method. The catalyst was further activated *in situ* through reduction by isopropyl alcohol (IPA), which served as both a hydrogen source and a reducing agent. Comprehensive structural, morphological, and compositional analyses confirmed the successful synthesis of the NiAl LDH material. The as-prepared catalyst was employed to carry out the CTH of benzaldehyde under external base-free conditions, using IPA as a green, readily available hydrogen donor. Benzaldehyde was selected as the model substrate due to its clean conversion to benzyl alcohol with high selectivity. Recyclability studies show interesting results, wherein, after the second cycle, a noticeable drop in product yield was observed, attributed to the leaching of Ni^{2+} ions, which serve as essential sites for IPA dehydrogenation. Post-recyclability characterization revealed a critical mechanistic transition, wherein the *in situ* reduction of Ni^{2+} ions progressively to metallic Ni^0 led to the emergence of a metal hydride-based reaction pathway in subsequent cycles. The newly formed Ni^0 particles act as active sites for IPA dehydrogenation, sustaining catalytic activity despite structural changes. Consequently, the CTH reaction evolves from a classical Lewis acid/base-mediated Meerwein–Ponndorf–Verley (MPV) mechanism to a hybrid pathway involving metallic Ni. Furthermore, the excellent green metric parameters associated with this protocol show its sustainability and practical applicability. Overall, this study demonstrates the potential of NiAl LDH as an efficient catalyst, capable of generating active Ni^0 sites under *in situ* conditions, thereby shifting the catalytic mechanism for the CTH of aromatic aldehydes. This work offers a promising strategy for green and scalable hydrogenation processes using non-noble metal catalysts and provides deeper insights into the underlying mechanisms.

2. Experimental section

2.1. Chemicals

Nickel nitrate hexahydrate (98%, Loba chemicals), aluminum nitrate nonahydrate (98%, Loba chemicals), sodium hydroxide (97.50%, Merck), sodium carbonate (SD fine), 1,1,2,2-tetrachloroethane (99%, SRL), isopropanol (99%, Fisher Scientific), *tert*-butyl alcohol (99%, SRL chemicals), bromothymol blue (SRL), phenolphthalein indicator (SDFCL), benzoic acid (99%, Tokyo Chemical Industry Co. Ltd), benzaldehyde (99%, SRL), 4-cyano benzaldehyde (98%, CDH), 4-bromo benzaldehyde (99%, Sigma Aldrich), 3-bromo benzaldehyde (>98%, TCI), and 2-nitro benzaldehyde (98%, Loba chemicals) were sourced commercially and utilized without undergoing any additional purification steps. High-purity deionized (DI) water, with a resistivity of 18.2 MΩ cm, was generated using a two-stage water purification system (ELGA PURELAB Option-R7). Deuterated chloroform ($CDCl_3$, 99.80%, Eurisotop) served as the solvent for NMR spectroscopy.

2.2. Synthesis of the nickel aluminum layered double hydroxide (NiAl LDH)

A facile co-precipitation method was applied for the synthesis of the nickel aluminum layered double hydroxide. The catalyst was synthesized in accordance with previous literature reports with minor modifications.[23,24] In brief, $Ni(NO_3)_2{\cdot}6H_2O$ (30 mmol) and $Al(NO)_3{\cdot}9H_2O$ (10 mmol) were dissolved in 100 mL of water. Then, a solution of NaOH and Na_2CO_3 was added dropwise to the metal salt solution with continuous vigorous stirring until the pH reached 10. This step was followed by the aging of the solution for 10 h at 70 °C. The as-obtained precipitates were then filtered and washed until the pH reached 7. Finally, the material was ground to get a fine powder of NiAl LDH after appropriate drying in a heating oven.

2.3. Catalytic transfer hydrogenation of benzaldehyde to benzyl alcohol

A simple hydrothermal method was employed for the CTH of benzaldehyde to benzyl alcohol using IPA as a green hydrogen donor. In a typical reaction, 1 mmol of benzaldehyde, 5 mL of IPA, and 50 mg of NiAl LDH were taken in a Teflon-lined hydrothermal vessel. Then, the vessel was kept in a stainless-steel hydrothermal reactor, which was then transferred to an electric oven and heated to a temperature of 190 °C for a period of 12 h. After the completion of the reaction, the catalyst was separated by centrifugation and was washed three times with acetone to recover the adsorbed reactants and products. The complete removal of the adsorbed species was confirmed by checking the TLC. After this, the resulting solution was concentrated by using a rotary evaporator. The yield of the product was calculated using the nuclear magnetic resonance (NMR) spectroscopic method, wherein, 1 mmol of 1,1,2,2-tetrachloroethane was used as an internal standard. The yield was calculated by integrating the area under the peaks of the benzylic protons of the product with respect to the protons of the internal standard. The formula used for the calculation of the NMR yield is shown in section S2. During the recyclability studies, after every cycle, the catalyst was characterized by PXRD and XPS. It was observed that during the reaction, some of the Ni^{2+} ions in the catalyst were *in situ* reduced to metallic Ni^0 particles.

3. Results and discussion

3.1 Synthesis and characterization studies

A facile method was opted for the synthesis of the NiAl LDH as shown in Scheme 1. The synthesis was carried out using metal salt precursors and basic solution. A particular pH was attained by using the base solution in order to completely precipitate the metals as their hydroxides. After attaining this pH, the solution was aged, followed by washing, drying, and finally grinding the catalyst. Also, during transfer hydrogenation reaction, the Ni^{2+} in NiAl LDH got *in situ* reduced to generate metallic Ni^0 particles dispersed on a layered matrix.

Powder X-ray diffraction analysis of NiAl LDH was carried out in order to investigate the crystal structure, and the results are presented in Fig. 1a. For NiAl LDH, the peaks in the PXRD plot were observed at angles of 11.53°, 23.31°, 35.10°, 39.38°, 47.36°, 60.15°, 62.28°, 66.14°, and 72.23° corresponding to the (003), (006), (012), (015), (018), (110), (113), (116) and (202) planes, respectively, matching well with the JCPDS No. 22-0700 corresponding to LDH.[25–29] Sharp peaks belonging to the brucite layer corresponding to the (003) plane with an interplanar distance of 7.69 Å are attributed the intercalation of CO_3^{2-} anions in between the layers.[30] The Fourier transform infrared (FTIR) spectra of the as-synthesized catalyst are presented in Fig. 1b. The broad band observed around 3300 cm^{-1} belongs to the O–H stretching vibrations of the surface hydroxyl groups and adsorbed water molecules.[31] A small peak belonging to the bending vibrations of water molecules can also be observed at 1625 cm^{-1}.[32] In addition, peaks belonging to the carbonate ions were observed at 795 cm^{-1} and 1354 cm^{-1}, which further verify the presence of carbonate in the interlamellar space. The results from PXRD and FTIR confirm successful intercalation of carbonate in the interlamellar space of NiAl LDH.[31–34] The peaks at 561 and 427 cm^{-1} are assigned to the M–O lattice vibrations.[35,36] Furthermore, the Raman spectrum (Fig. 1c) shows the presence of peaks related to different vibrational modes. The peaks at 149 cm^{-1}, 448 cm^{-1}, 550 cm^{-1}, and 1048 cm^{-1} correspond to M–O stretching vibrations, bending vibrations of Ni–OH and Al–O, and vibrations from CO_3^{2-} ions, respectively.[37,38] Thermogravimetric analysis (TGA) and Derivative Thermogravimetry (DTG) were carried out to investigate the

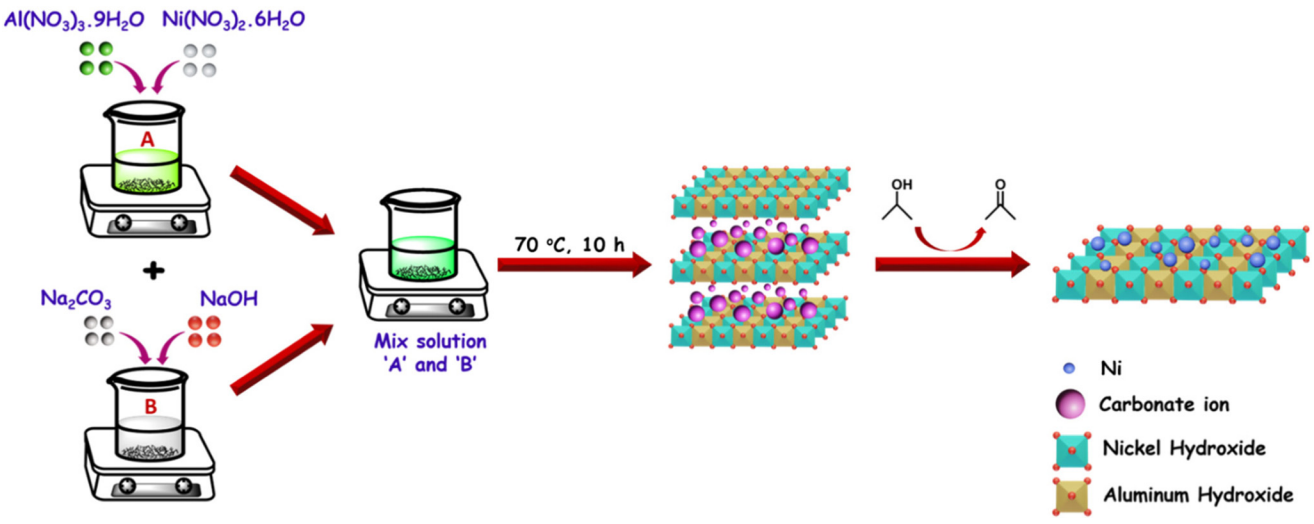

Scheme 1 Schematic representation of the synthesis of NiAl LDH followed by *in situ* reduction of Ni^{2+} to Ni^0 during the transfer hydrogenation reaction.

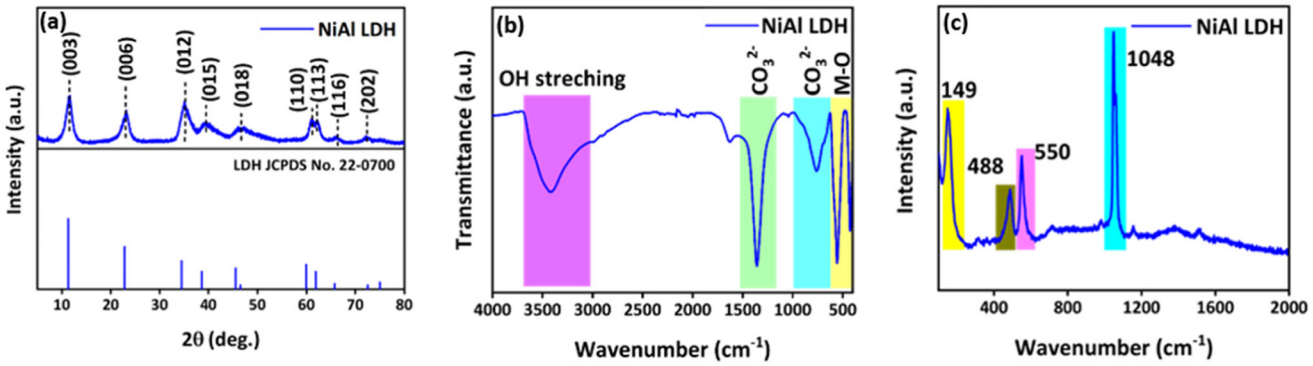

Fig. 1 (a) PXRD pattern of NiAl LDH, (b) FTIR spectrum of NiAl LDH and (c) Raman spectrum of NiAl LDH.

thermal stability of the NiAl LDH. The results of thermal analysis are shown in Fig. S1. Here, two major weight loss regions can be seen, *i.e.* in the temperature ranges (i) 25 °C to 190 °C and (ii) 190 °C to 380 °C and 380 °C to 500 °C.[39,40] The first major weight loss occurs from 25 °C to 190 °C accounting for a reduction in weight by 13%. This could further be sub-divided into three distinct regions *i.e.* (a) from 25 °C to 100 °C attributed to the loss of weakly adsorbed water molecules on the surface and (b) from 100 °C to 190 °C attributed to the loss of water molecules present in the interlayer space of NiAl LDH.[39,40] The second major weight loss in the region of 190 °C to 360 °C may be attributed to the decomposition of the carbonate anions. The third major weight loss in the region of 380 °C to 500 °C occurred due to the decomposition of the surface hydroxyl groups.[39,41] This weight loss leads to the destruction of the LDH structure and its conversion to the corresponding mixed metal oxide.[41] Until 580 °C, a total reduction in weight by 37% was observed. After 580 °C, no significant weight loss was observed, indicating high stability of the formed mixed metal oxide.

In addition, scanning electron microscopy (SEM) analysis was carried out to investigate the morphology of the as-synthesized NiAl LDH catalyst. The SEM images are presented in Fig. 2a and b, which show the presence of agglomerated platelet-like structures of variable sizes. Furthermore, transmission electron microscopy (TEM) images, as depicted in Fig. 2c and d, also confirm the presence of flake-like structures in the material. Besides, the high-resolution transmission electron microscopy (HR-TEM) image in Fig. 2e shows the presence of lattice fringes with the *d*-spacing of 0.19 nm corresponding to the (018) plane.[42] Alongside this, the inverse fast Fourier transform (IFFT) with FFT in the inset and line profiling of this image are shown in Fig. 2f and g, respectively. As shown in Fig. 2h, the energy-dispersive analysis (EDAX) of NiAl LDH reveals the presence of Ni, Al, O, and C in the material. SEM elemental mapping (Fig. 2i–m) was carried out in order to investigate the distribution of various elements in NiAl LDH and the results confirmed their homogeneous distribution.

Furthermore, X-ray photoelectron spectroscopy (XPS) was employed to gain better insights into the oxidation states, bonding environment, and elemental composition of the NiAl LDH catalyst. Fig. S2a shows the XPS survey spectrum of the NiAl LDH. The Ni 2p high-resolution spectrum (Fig. 3a) shows characteristic peaks at 855.39 and 872.94 eV corresponding to Ni^{2+} $2p_{3/2}$ and $2p_{1/2}$ and peaks at 857.91 and 875.48 eV corresponding to Ni^{3+} $2p_{3/2}$ and $2p_{1/2}$, respectively.[26,43–45] Additional peaks observed at 882.08, 879.13, 864.87, and 861.50 eV correspond to the satellite peaks of Ni. Furthermore, the Al 2p high-resolution spectrum (Fig. 3b) can be deconvoluted into two peaks at 73.8 and 68.2 eV, belonging to Al^{3+} 2p and Ni^{2+} 3p.[46,47] The O 1s high resolution spectrum (Fig. 3c) shows the presence of three peaks at binding energies of 529.9, 531.4, and 532.8 eV belonging to the M–O–M bond, M–O–H bond and the interlayer adsorbed water, respectively.[46,48] Finally, the C 1s high resolution spectrum (Fig. 3d) can be deconvoluted into three distinct peaks, *viz.* 284.8, 286.3, and 288.6 eV, attributable to the surface-adsorbed carbon, C–O and the carbon from the carbonate ion, respectively.[49] Furthermore, the atomic percentages of O, Ni, C, and Al on the surface of the catalyst as determined by XPS studies were found to be 56.17, 18.22, 19.18, and 6.43%, respectively, as shown in Fig. S2b.

The Brunauer–Emmett–Teller (BET) analysis was carried out in order to calculate the specific surface area of the material.[50] Although LDHs typically exhibit low specific surface areas, the surface area of the NiAl catalyst is comparatively higher than those of some of the other reported non-noble metal-based catalysts, which contributes to its enhanced catalytic activity.[51,52] The N_2 desorption isotherm, Barrett–Joyner–Halenda (BJH) pore size and multi-point BET plots of NiAl LDH are shown in Fig. 4. The NiAl LDH exhibits a type IV isotherm with a prominent H3-type hysteresis loop (Fig. 4a).[50,53] Also, the BJH pore size distribution curve (Fig. 4b) revealed the presence of mesopores in NiAl LDH with an average pore size of 3.8 nm and a pore volume of 0.39 cm^3 g^{-1}. Multi-point BET (Fig. 4c) was employed to calculate the surface area of the NiAl LDH material, which was found to be 78 m^2 g^{-1}. In addition, the organic acid titration method was used to determine the basic sites in the material. The total basicity was determined by using bromothymol blue as an

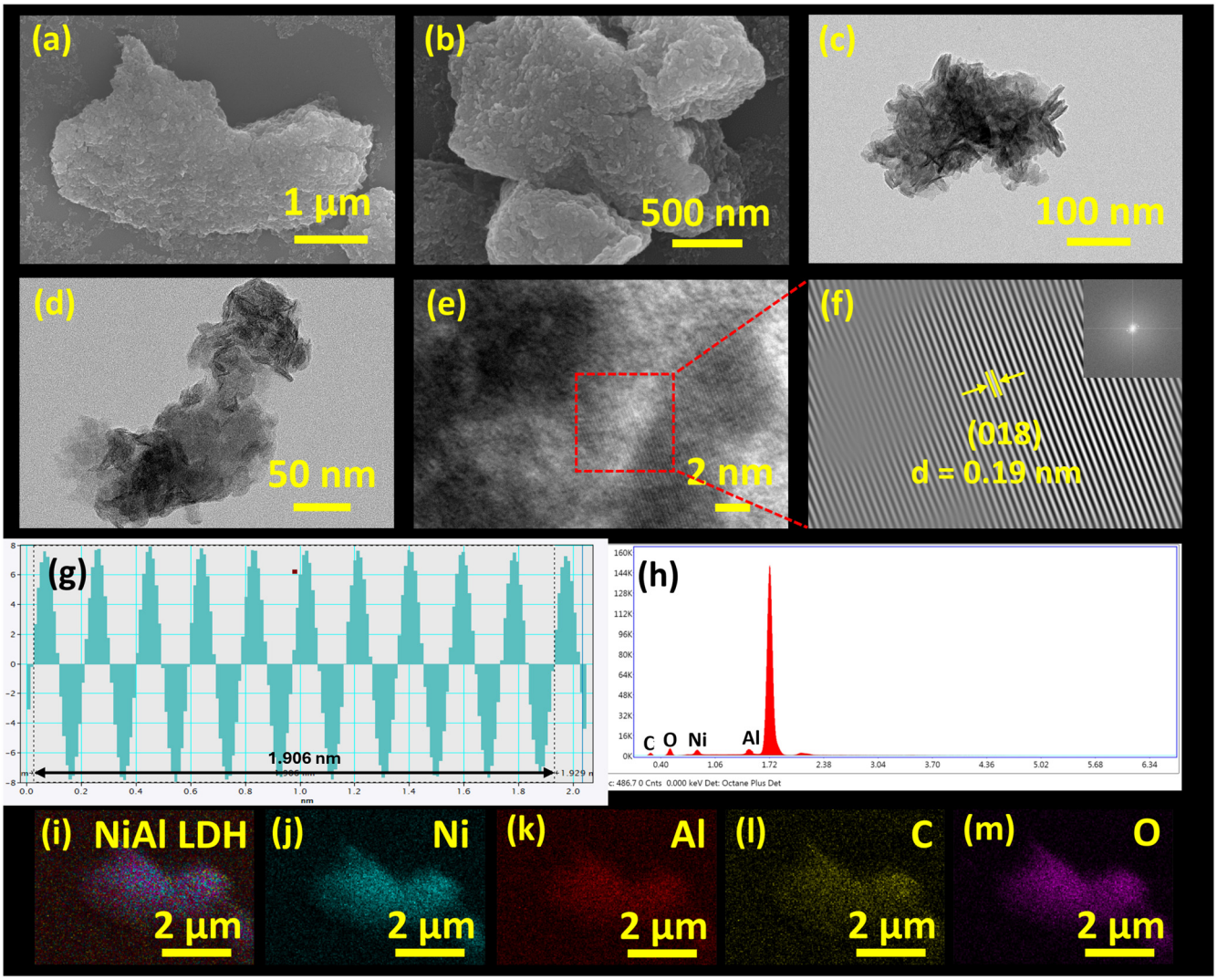

Fig. 2 (a and b) SEM images, (c and d) TEM images, (e) HR-TEM image, (f) IFFT (inset FFT), (g and h) EDAX spectra and (i–m) elemental mapping of NiAl LDH.

indicator and benzoic acid as a titrant. Typically, 50 mg of catalyst was added to 5 mL of 2×10^{-5} M bromothymol blue solution. The solution was stirred for about 30 min and then titrated against 0.01 M benzoic acid solution. A color change from yellow to blue was observed with the addition of a catalyst to the indicator solution (Fig. S3). The basicity was calculated based on the formula given in section S3, and was 0.5 mmol g^{-1}.

3.2. Catalytic activity studies

A facile protocol was developed for the evaluation of the catalytic activity of the NiAl LDH catalyst for CTH under base-free conditions. Benzaldehyde was chosen as the model substrate, and IPA was utilized as a green hydrogen source for the CTH process. Detailed optimizations were carried out by varying reaction parameters like catalyst amount, temperature, time of reaction, and hydrogen source. Initially, the amount of catalyst was optimized to achieve maximum conversion of benzaldehyde. Fig. 5a shows the effect of a change in the amount of catalyst on the yield of benzyl alcohol. When the reaction was carried out using 20 mg of catalyst, a 78% yield of benzyl alcohol was obtained. The yield of benzyl alcohol increased to 94% on increasing the amount of catalyst to 50 mg. This increase in the yield of product was observed due to an increase in the number of catalytically active sites with an increase in catalyst amount. Keeping these results in consideration, the amount of catalyst was fixed to 50 mg, and further optimizations were carried out by varying other parameters.

In order to check the effect of temperature on the yield of benzyl alcohol, further optimizations were carried out. As shown in Fig. 5b, a gradual increase in the yield of benzyl alcohol from 80% to 94% was observed when the temperature increased from 160 °C to 190 °C. The increase in the reaction temperature leads to more reactant molecules crossing the energy barrier and getting converted into the products. After

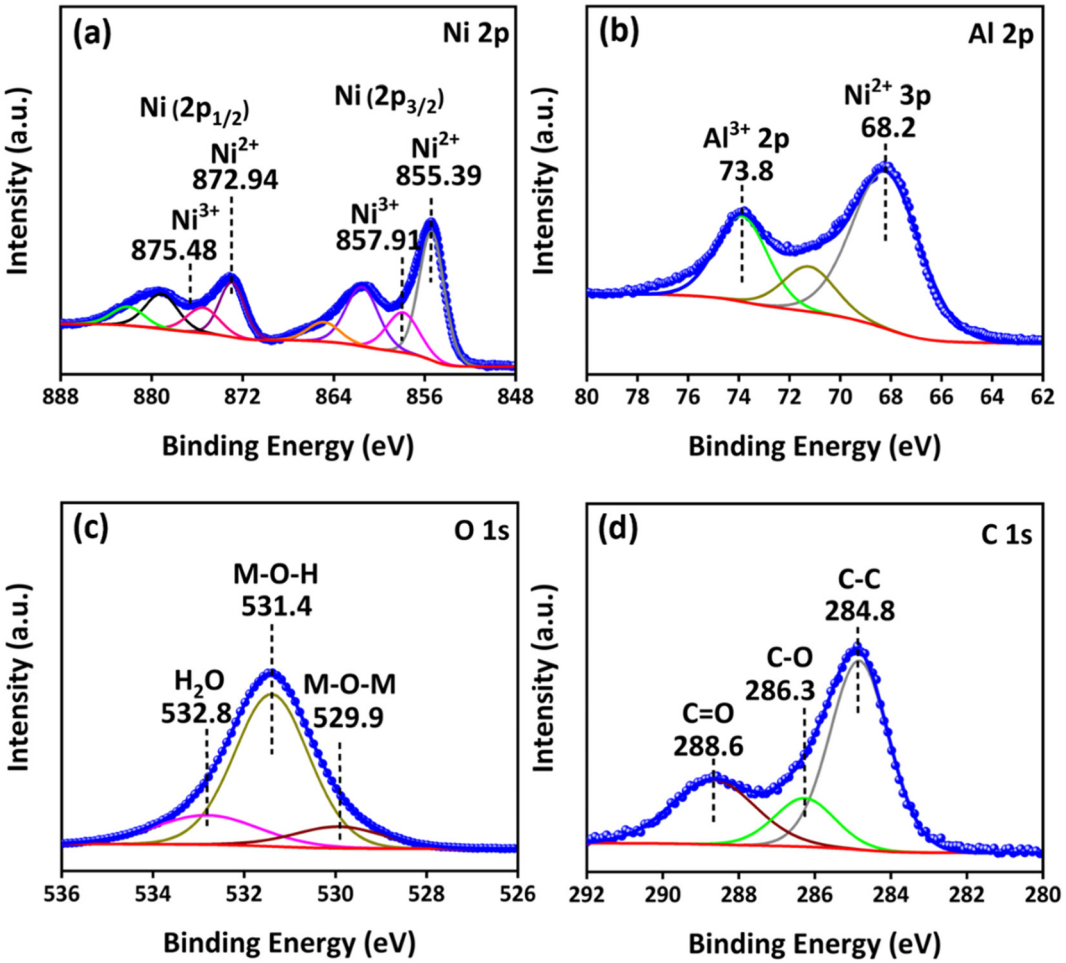

Fig. 3 XPS spectra of (a) Ni 2p, (b) Al 2p, (c) O 1s and (d) C 1s of the NiAl LDH catalyst.

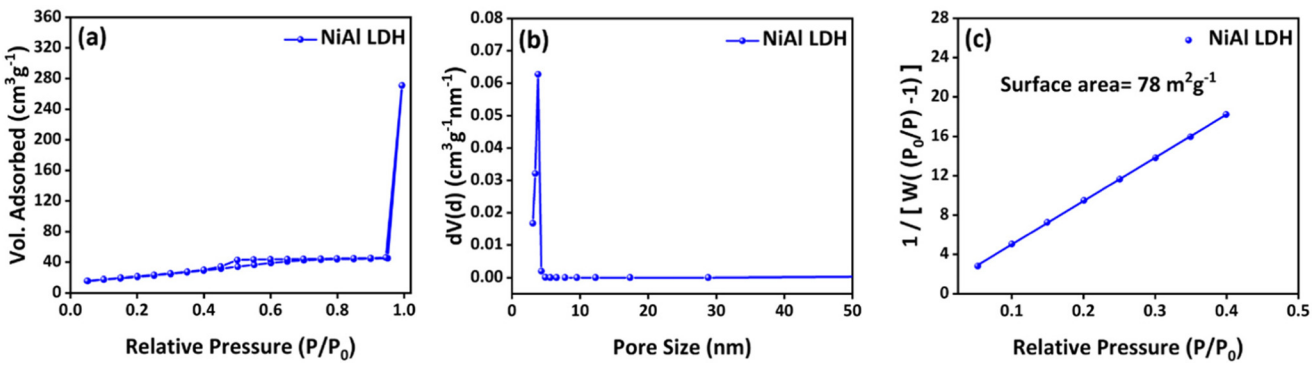

Fig. 4 (a) BET plot of N_2 adsorption–desorption isotherms, (b) BJH pore size distribution plot, and (c) surface area plot of NiAl LDH.

that, the reaction time was examined as shown in Fig. 5c, and a significant increase in the yield of product, *i.e.*, from 79% to 94%, was observed when the time of reaction was increased from 6 h to 12 h. Then, the performance of the catalyst for the CTH of benzaldehyde was evaluated using different hydrogen sources (Fig. 5d). Optimizations using different hydrogen sources were carried out, and it was observed that the reaction carried out using methanol as a hydrogen source gave the lowest yield of benzyl alcohol *i.e.*, 28%. Meanwhile, the yields of benzyl alcohol using 2-butanol, ethanol and IPA were 72, 86, and 94%, respectively. These results show that the hydrogen donating ability of secondary alcohol (isopropyl alcohol) is much greater than that of primary alcohols (ethanol and methanol). This occurs due to the following reasons: (i) IPA

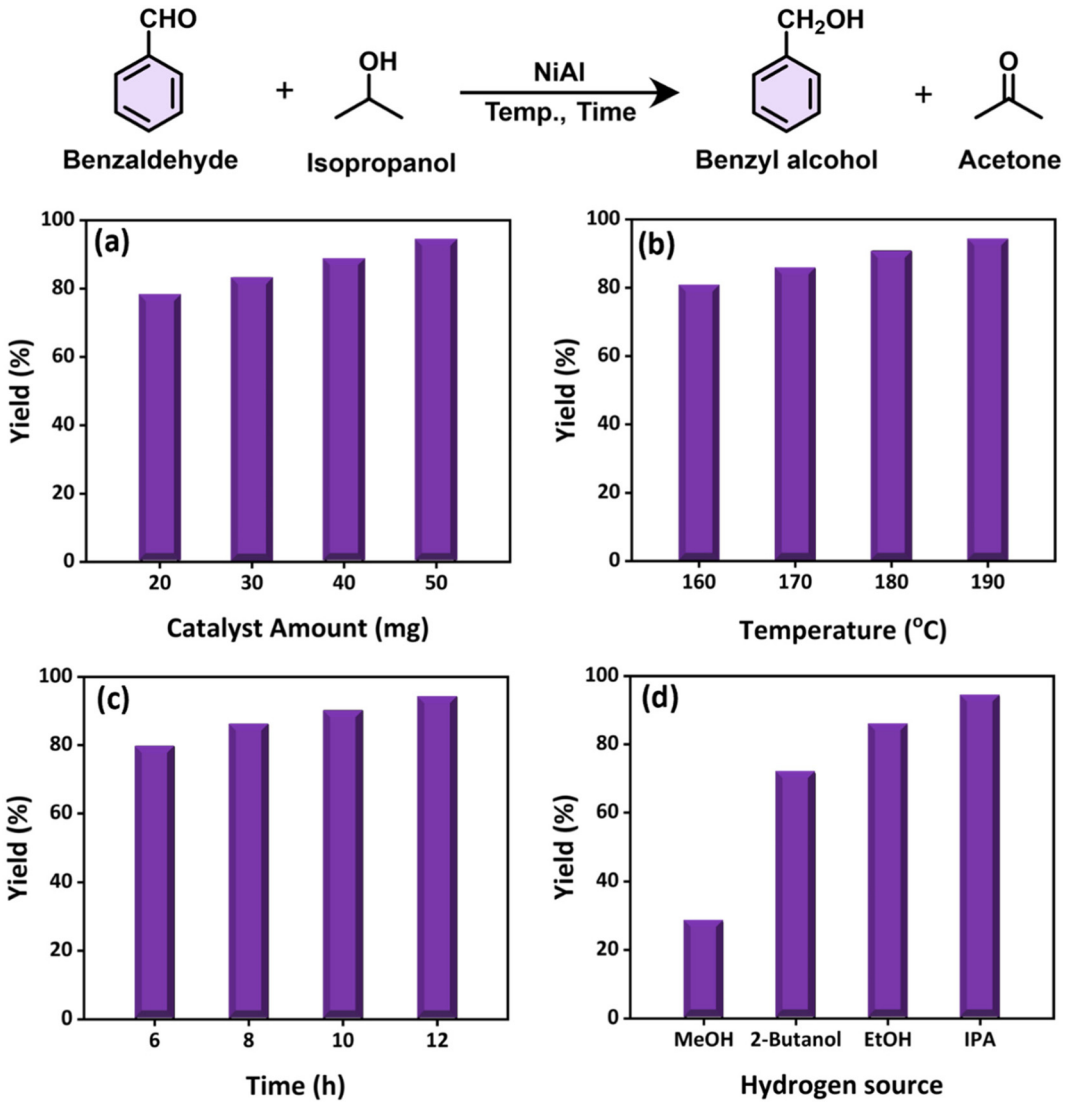

Fig. 5 Optimization of reaction conditions for the transfer hydrogenation of benzaldehyde using NiAl LDH: (a) variation in catalyst amount (reaction conditions: IPA (5 mL), time (12 h), and temperature (190 °C)); (b) variation in reaction temperature IPA (5 mL), catalyst amount (50 mg), and time (12 h); (c) variation in reaction time (reaction conditions: IPA (5 mL), catalyst amount (50 mg), and temperature (190 °C)); (d) variation in the hydrogen source (reaction conditions: catalyst amount (50 mg), time (12 h), temperature (190 °C), and hydrogen source (5 mL)).

being a secondary alcohol has a weaker –OH bond as compared to other hydrogen sources, (ii) more α-hydrogens are present in IPA as compared to other hydrogen sources, and (iii) IPA has a lower reduction potential as compared to primary alcohols.[54] Interestingly, 2-butanol as a hydrogen source gave a lower yield of benzyl alcohol as compared to that obtained using ethanol. This can possibly be attributed to the steric factors that become significant in 2-butanol. Furthermore, a control reaction in the absence of a catalyst gave benzyl alcohol in 11% yield only.

The designed protocol of the CTH reaction was further applied to substituted aromatic aldehydes (Scheme 2). It was observed that the reaction proceeded well for both electron-donating and electron-withdrawing substituents giving high yields of the corresponding alcohols. Also, it was observed that the yield of alcohol was high irrespective of the position to which the substituent was attached. Furthermore, when benzophenone was used as a model substrate to investigate the applicability of the designed protocol to aromatic ketones, it was observed that the ketone group remained unaffected. This is due to the fact that ketones are less electrophilic, sterically hindered and generally require harsh conditions to get hydrogenated.[55] Additionally, substrates with reduction-prone groups, *viz.* nitro and cyano, remained unaffected, indicating high selectivity of the designed protocol towards the aldehyde group.

A detailed comparison of the performance of our employed catalyst with other reported catalysts for hydrogenation of benzaldehyde has been mentioned in Table S1. The methodology developed in this work employs NiAl LDH for transfer

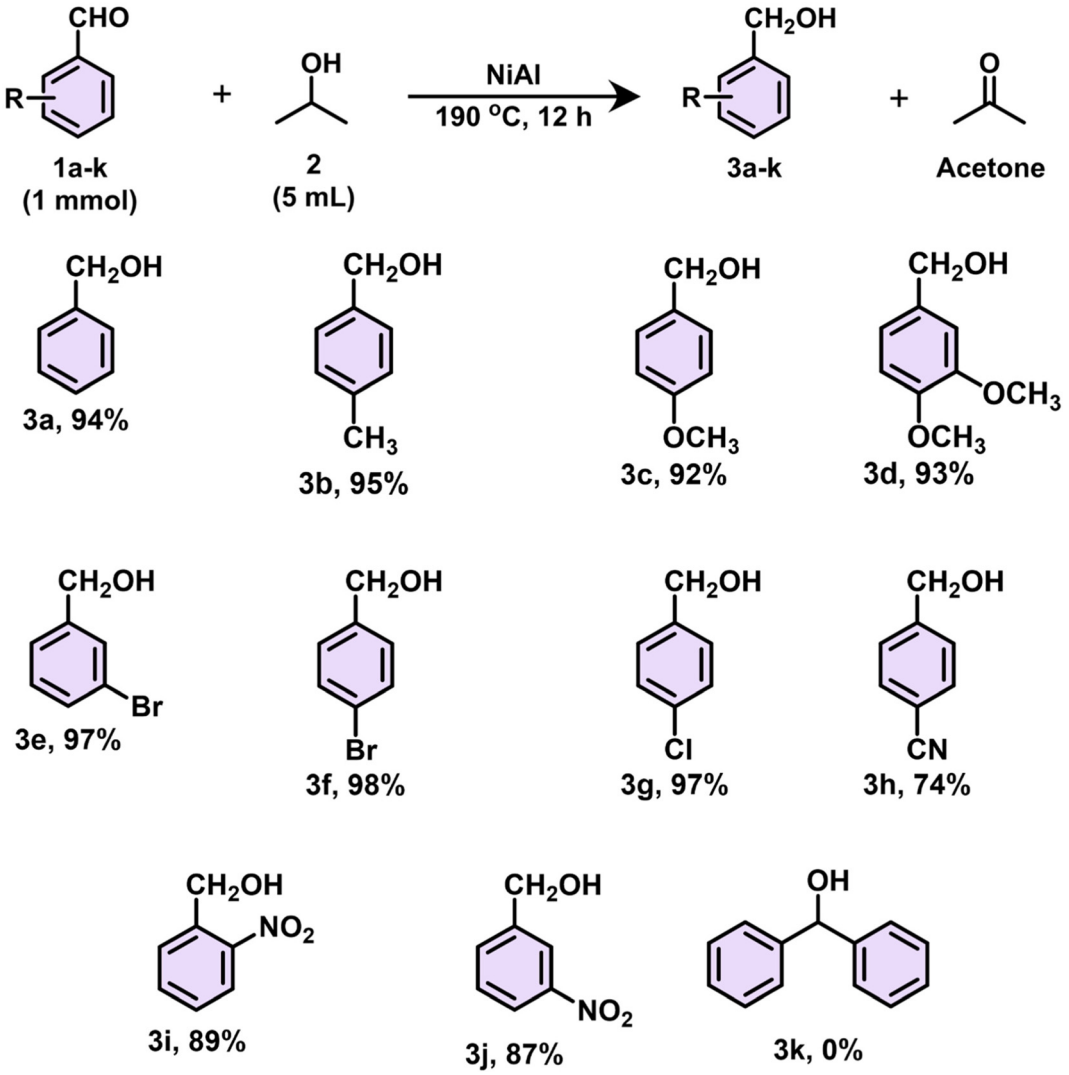

Scheme 2 Transfer hydrogenation of different aromatic aldehyde substrates. NMR yield is reported using 1,1,2,2-tetrachloroethane as an internal standard.

hydrogenation of benzaldehyde under optimized reaction conditions. The facile synthesis conditions provide some advantages over those of other reported catalysts for scaling up from an industrial point of view. In earlier reports, hydrogenation of benzaldehyde has been carried out using both heterogeneous and homogeneous catalysts. The homogeneous catalysts generally employ noble metals, face thermal stability issues, and are difficult to recover. On the other hand, the reported heterogeneous catalysts use a base as an additive. The addition of the base in a reaction raises the concern of environmental friendliness of the process. There are several reports in the literature where hydrogenation of benzaldehyde has been carried out using molecular hydrogen as well. Molecular hydrogen has to be used under high pressure and is highly flammable, raising safety concerns. Also, its operation requires sophisticated equipment, thus raising the overall costs of the process. Thus, the protocol developed in this work is highly efficient for the hydrogenation of benzaldehyde. However, the temperature required for the developed reaction protocol is higher than those of other catalytic systems presented in Table S1.

3.3. Recyclability studies

One of the most important and distinguishing features of heterogeneous catalysts compared to homogeneous catalysts is their recyclability. To evaluate the stability of the catalyst, recyclability studies were conducted over four consecutive reaction cycles under optimized reaction conditions. The results are presented in Fig. 6a. During these studies, it was observed that the product yield remained excellent up to the second cycle. However, a noticeable decrease in yield was observed after the second cycle. In the fourth cycle, the yield remained comparable to that of the third cycle, with no further significant decline.

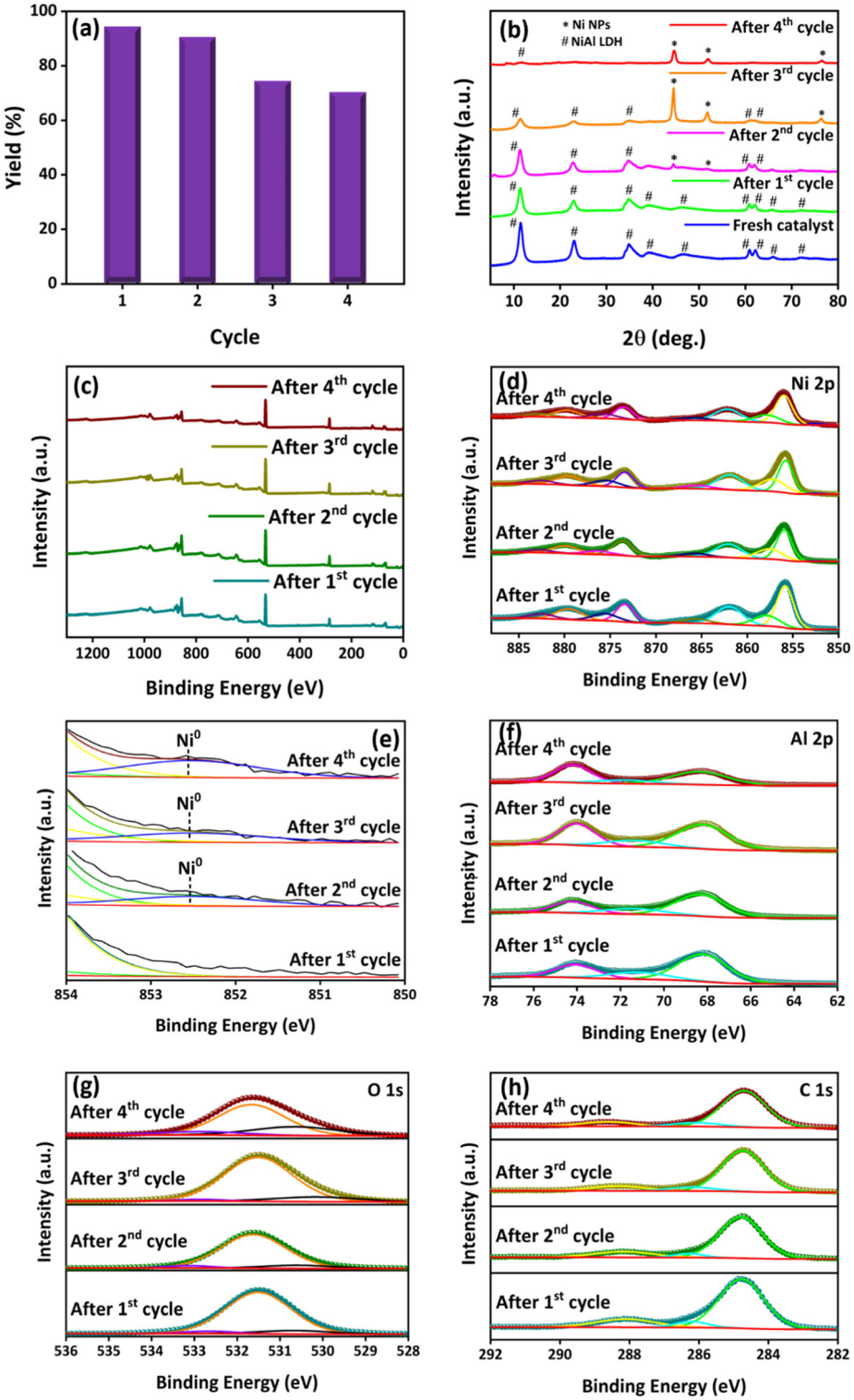

Fig. 6 (a) Recyclability study of NiAl LDH, (b) PXRD plots after each catalytic cycle, (c) XPS survey spectra, XPS spectra of (d) Ni 2p, (e) zoomed version of Ni 2p high resolution XPS spectra, and XPS spectra of (f) Al 2p, (g) O 1s, and (h) C 1s of spent catalysts.

To investigate the cause of the decreased yield after the second cycle, detailed structural and compositional analyses were performed using PXRD and XPS. The PXRD analysis of the recovered catalyst after each cycle is shown in Fig. 6b. After the second cycle, a diffraction plane corresponding to the (111) plane of Ni appeared. By the fourth cycle, the diffraction peaks associated with metallic Ni^0, specifically the (111), (200), and (220) planes, became more intense compared to the peaks

of the NiAl LDH phase, indicating that the catalyst had largely transformed into metallic Ni^0 supported on the LDH-derived matrix. The diffraction peaks of the LDH-derived matrix are not visible in the PXRD plot due to its amorphous nature and their much lower intensity compared to the Ni^0 diffraction planes. This transformation can be attributed to the *in situ* reduction of Ni^{2+} to Ni^0 during the transfer hydrogenation of aldehydes, with isopropanol (IPA) acting as both the hydrogen source and reducing agent. To confirm the formation of metallic nickel particles, TEM was performed. TEM images (Fig. S4a and b) show the presence of metallic nickel particles. Furthermore, the HRTEM image, inverse fast Fourier transform (IFFT) image along with fast Fourier transform (FFT) image and line profiling of the recovered catalyst (Fig. S4c–e) show lattice fringes with a *d*-spacing of 0.20 nm corresponding to the (111) plane, which is in accordance with the PXRD results. This observation is consistent with a previous report, where Pan *et al.*[7] had reported *in situ* reduction of Cu^{2+} to Cu^+ and Cu^0 using IPA, wherein the reduced Cu^0 atoms nucleate and grow into nanoparticles dispersed on the LDH support.

Additionally, XPS analysis of the recovered catalysts after each cycle is shown in Fig. 6c–h. A zoomed version of high-resolution Ni 2p spectra shows the emergence of peaks around 852.5 eV, corresponding to the $2p_{3/2}$ level of Ni^0, starting from the second cycle (Fig. 6e). Also, a significant decrease in Ni content was observed from 18.22% in the fresh catalyst to 5.72% after the fourth cycle (Table 1). The Ni^{2+} to Ni^0 ratio also indicated an increase in Ni^0 content from the second to fourth cycle, changing from 1 : 0.02 to 1 : 0.05 (Table 1). Based on these structural and compositional analyses, the decline in recyclability was mainly attributed to Ni leaching from the catalyst as evidenced from the decreased Ni content in the recovered catalyst. However, the stable yields observed in the third and fourth cycles were due to the *in situ* formation of metallic Ni^0, which remained catalytically active. Therefore, it was concluded that in these cases, metallic Ni^0 serves as the active species responsible for transfer hydrogenation of aldehydes to their corresponding aromatic alcohols in the later cycles. Moreover, due to the formation of the metallic Ni^0, the reconstruction of the NiAl LDH is not possible. Moreover, the carbon content after the fourth cycle is higher than that of the fresh catalyst, even though the catalyst undergoes decarboxylation during the transformation of NiAl-LDH to Ni-Al_2O_3. This increase in carbon content may be attributed to carbon deposition on the surface of the catalyst, which can block the catalytically active sites for subsequent cycles.

3.4. Structure–activity correlation and mechanism of reaction

To better understand the roles of acidic and basic sites in the catalytic transfer hydrogenation (CTH) process, poisoning experiments were conducted, as illustrated in Scheme S1. In these studies, pyridine and benzoic acid were employed as selective poisons for the acidic and basic sites of the NiAl LDH catalyst, respectively. Pyridine acts as a Lewis base that preferentially coordinates to acidic sites and hampers their activity. In contrast, benzoic acid, a Brønsted acid, interacts with basic sites and hampers the activity of the catalyst. When pyridine was introduced to quench the acidic sites, the yield of benzyl alcohol dropped to 78%, indicating a partial inhibition of the reaction. However, when benzoic acid was used to poison the basic sites, the product yield declined significantly to 29%. This substantial decrease highlights the crucial role of basic sites in facilitating the CTH of benzaldehyde to benzyl alcohol. These observations suggest that although both acidic and basic sites are involved in the reaction mechanism. The basic sites on the NiAl LDH catalyst play a more dominant role in the catalytic process. The significant impact of basic site quenching implies that they may be directly responsible for activating the hydrogen donor (*e.g.*, isopropanol) or facilitating the adsorption and transformation of the aldehyde substrate. Overall, the poisoning experiments show the importance of maintaining the acid–base balance on the catalyst surface and affirm that the basic sites are essential for achieving high efficiency in the CTH of benzaldehyde.

The transfer hydrogenation of aldehydes to the corresponding alcohols involves two reaction pathways *i.e.*, Meerwein–Ponndorf–Verley (MPV) and metal hydride mediated reaction pathways as depicted in Scheme 3. Based on the aforementioned characterization and experimental findings, these reaction mechanisms were proposed for the catalytic transfer hydrogenation (CTH) of benzaldehyde to benzyl alcohol. Drawing upon insights from previous literature,[6,56–58] we propose that the Meerwein–Ponndorf–Verley mechanism governs the initial CTH process using the fresh NiAl LDH catalyst. This classical mechanism is typically facilitated by the synergistic interaction of Lewis-acidic (Ni^{2+}/Al^{3+}) and Lewis-basic (O^{2-}) sites inherent in the layered double hydroxide (LDH) framework.

The MPV-type mechanism progresses through the formation of a six-membered cyclic transition state (Scheme 3a).[58,61] In the first step (i), the benzaldehyde and isopropanol adsorb onto the catalytically active surface of the

Table 1 Table showing the atomic percentage of constituent elements for fresh and recovered catalysts

S. no.	Element	Fresh catalyst	After 1st cycle	After 2nd cycle	After 3rd cycle	After 4th cycle
1	Ni 2p	18.22	13.66	12.54	6.89	5.72
2	Al 2p	6.43	5.64	5.90	30.98	26.4
3	O 1s	56.17	50.78	48.18	36.98	37.09
4	C 1s	19.18	29.92	33.38	25.15	30.79
5	Ni^0 to Ni^{2+}	—	—	2.00	3.00	5.00

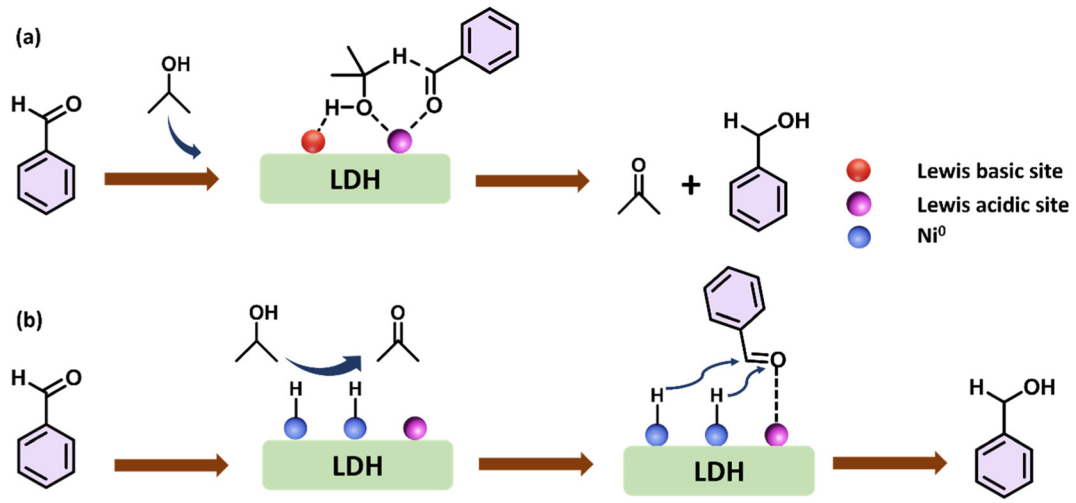

Scheme 3 Plausible reaction mechanisms for the CTH of benzaldehyde to benzyl alcohol in the presence of IPA using NiAl LDH: (a) Meerwein–Ponndorf–Verley (MPV) mediated pathway and (b) metal hydride mediated pathway.

NiAl LDH. The oxygen atom of the alcohol coordinates with the Lewis-acidic metal centres (preferably Ni^{2+}), while the hydroxyl hydrogen interacts with the Lewis-basic O^{2-} species of the LDH which play a crucial role as confirmed from the structure–activity correlation studies. Simultaneously, the carbonyl group of benzaldehyde also coordinates with the Lewis-acidic sites, positioning the molecules favourably for hydride transfer. In the second step (ii), a six-membered cyclic transition state forms, bringing the hydride donor (isopropanol) and the carbonyl acceptor (benzaldehyde) in close proximity. In the third step (iii), a concerted hydride transfer occurs: the α-hydrogen of isopropanol is transferred to the carbonyl carbon of benzaldehyde, resulting in the formation of benzyl alcohol and acetone. This step involves simultaneous bond breaking and bond formation. Finally, in step (iv), the products desorb from the catalyst surface, thereby regenerating the active sites and completing the catalytic cycle.

In addition to the MPV mechanism, an intriguing phenomenon was observed during the recyclability studies of the catalyst. As the number of cycles increased in the recyclability studies, the Ni^{2+} species in the NiAl LDH were gradually reduced to metallic Ni^0 particles due to the *in situ* reducing environment provided by isopropanol. This reduction was confirmed through PXRD and XPS analyses, which revealed a progressive increase in the Ni^0 content after each cycle. Consequently, with the formation of metallic Ni particles, the mechanism of the CTH reaction began to shift from the MPV pathway to a metal-hydride pathway, as depicted in Scheme 3b.[7] In this alternative pathway, the dehydrogenation of isopropanol is facilitated by both the metallic Ni^0 particles and the Lewis-acidic (Ni^{2+} and Al^{3+}) sites of the catalyst. Isopropanol undergoes dehydrogenation to form a metal hydride species on the surface of the Ni particles. The resulting hydride is then transferred to the carbonyl carbon of benzaldehyde to form benzyl alcohol as a product. This mechanistic shift explains the sustained catalytic activity observed in the third and fourth reaction cycles, even as the original NiAl LDH structure was lost. Thus, while the MPV mechanism dominates in the initial reaction cycles with the fresh catalyst, the metal-hydride pathway becomes prominent in the subsequent cycles due to the structural evolution of the catalyst.

3.5. Green metric parameters

Green metric parameters were calculated for the transfer hydrogenation of benzaldehyde to form benzyl alcohol (section S4).[59–61] The calculated values of different parameters are shown in Table 2. During the reaction, acetone is formed in an equimolar amount; however, it evaporates during the reaction workup on account of its low boiling point. Therefore, acetone is not considered a byproduct but is treated as waste in the green metric calculations. Here, the environmental factor (EF) emphasizes the waste generated in the reaction and a small value of EF indicates minimal waste generation during the reaction and the process being more sustainable. The EF for our developed protocol was calculated as 0.644. Furthermore, we also calculated the EF for reactions attempted using different hydrogen sources. The EF values were calculated as 0.652 for ethanol, 1.337 for 2-butanol, and 3.6 for

Table 2 Summary of green metric parameters for the CTH of benzaldehyde to benzyl alcohol

S. no.	Green metric parameter	Ideal value	Obtained value
1	Environmental factor (EF)	0	0.644
2	Atom economy (AE)	100%	65%
3	Process mass intensity (PMI)	1	40
4	Carbon economy	100%	70%
5	Solvent intensity (SI)	0	0
6	Renewable intensity (RI)	Higher is better	39
7	Renewable percentage (RP)	100%	98%
8	Reaction mass efficiency (RME)	100%	66%
9	Mass intensity (MI)	1	40

methanol. Furthermore, atom economy (AE) is related to the synthetic efficiency of the applied reaction protocol and gives the idea of the number of atoms of reactants that were incorporated into the products. Our designed protocol had an AE value equal to 65%, indicating that the majority of the atoms of the reactants were incorporated into the product (benzyl alcohol). It is noteworthy to mention here that the byproduct (acetone) formed during this reaction was neither isolated nor quantified due to practical issues in its isolation. Another parameter of utmost importance is process mass intensity (PMI), which refers to the mass of raw materials utilized for obtaining products.[62] It can also be calculated from the EF (PMI = EF + 1). PMI is calculated as the ratio of the total mass of reactants (including solvent) to the mass of the product in the process. Ideally, the value of PMI is 1 which suggests that the input and output are equal, leaving no waste or unreacted components. In our case the value of PMI is 40. The high value of PMI was due to the excess IPA used for transfer hydrogenation reaction. It is noteworthy to mention that IPA is a green solvent, and the excess amount used can be recovered using fractional distillation.

Carbon economy (CE) refers to the ratio of the carbon in the product to that present in the reactant and is usually expressed in percentage.[63] The carbon economy for our process came out to be 70%. The solvent intensity (SI) quantifies the amount of product used with respect to the solvent.[63] For any process to be suitable for the industry, the amount of solvent used in a chemical process should be low, minimizing the overall cost of the productivity. A higher solvent intensity indicates a high level of solvent waste, which must be treated or disposed of, ultimately adding to the environmental footprint of a process. Since no additional solvent is involved in the reaction, the value for solvent intensity is 0. The renewable intensity (RI) parameter is used to estimate the proportion of renewable materials in comparison with total resources consumed in a process.[64] The renewable intensity for our developed protocol turned out to be 39. The higher value of renewable intensity signifies that most of the raw materials used during the process are derived from renewable sources. The renewable percentage (RP) was calculated.[64] The RP is used to quantify the percentage of renewable resources used in a process relative to the total resources used. For our protocol, the value of renewable percentage was 96%. Reaction mass efficiency (RME) is defined as the percentage mass of the target product with respect to the mass of all reactants.[65] A value of 66% was obtained for our reaction. Mass intensity (MI) helps to estimate the total mass of all materials used to produce one unit of product.[63] A sustainable process tends to have a lower value of mass intensity. Our strategy has a MI value of 40.

4. Conclusions

In this work, we present a robust and environmentally benign strategy for the catalytic transfer hydrogenation (CTH) of benzaldehyde using isopropanol (IPA) as a green hydrogen source. A key highlight of this study is the *in situ* generation of active Ni^0 species from a NiAl layered double hydroxide (LDH) precursor during the reaction process. This transformation not only drives the reduction of benzaldehyde to benzyl alcohol under base-free conditions but also fundamentally alters the reaction pathway upon catalyst reuse. Initially, the reaction proceeds *via* a classical Meerwein–Ponndorf–Verley (MPV) mechanism. However, after the second catalytic cycle, structural and compositional analyses reveal a progressive reduction of Ni^{2+} to Ni^0, driven by IPA as a reducing agent under the reaction conditions. The resulting Ni^0 particles shift the catalytic mechanism from the MPV to a metal-hydride pathway, wherein dehydrogenation of IPA occurs over the metallic Ni surface, assisted by the remaining Lewis acid sites, followed by the hydrogenation of the aldehyde to yield the corresponding alcohol. This dual mechanistic pathway explains the sustained catalytic activity in later cycles, despite the transformation of the original LDH structure. Furthermore, control and poisoning experiments highlight the crucial role of basic sites in the initial MPV-type CTH process. The developed protocol also demonstrates excellent substrate scope and high chemoselectivity, particularly towards aldehyde groups, leaving reducible nitro and ketone functionalities unaffected under the optimized conditions. Overall, this study not only introduces a facile and scalable route for the *in situ* synthesis of metallic Ni particles but also provides insights into an effective catalytic system wherein the structural evolution of the catalyst induces a mechanistic shift, enhancing the sustainability of the process.

Conflicts of interest

There are no conflicts to declare.

Data availability

The data supporting this article have been included as part of the supplementary information (SI). Supplementary information: material characterization, yield calculations, TGA-DTG plot, XPS survey spectra and atomic percentage table of NiAl LDH, titration images, basicity calculations, comparison table, control reactions, green metric calculations, post-recyclability TEM data, compound characterizations and NMR data of different substrates. See DOI: https://doi.org/10.1039/d5dt02279g.

Acknowledgements

We are thankful to the Advanced Materials Research Center (AMRC), IIT Mandi, for laboratory and characterization facilities. AS thanks the Ministry of Education (MoE), Government of India, for the doctoral fellowship. SK and DS thank the Ministry of Education (MoE), Government of India, for the Prime Minister's Research Fellowship.

References

1 J. T. Bhanushali, I. Kainthla, R. S. Keri and B. M. Nagaraja, *ChemistrySelect*, 2016, **1**, 3839–3853.
2 W. Johnson, W. F. Bergfeld, D. V. Belsito, R. A. Hill, C. D. Klaassen, D. C. Liebler, J. G. Marks, R. C. Shank, T. J. Slaga and P. W. Snyder, *Int. J. Toxicol.*, 2017, **36**, 5S–30S.
3 B. Nair, *Int. J. Toxicol.*, 2001, **20**, 23–50.
4 H. Shoukat, A. A. Altaf, M. Hamayun, S. Ullah, S. Kausar, M. Hamza, S. Muhammad, A. Badshah, N. Rasool and M. Imran, *ACS Omega*, 2021, **6**, 19606–19615.
5 H. M. Lapa and L. M. Martins, *ACS Omega*, 2024, **9**, 26780–26804.
6 D. Sharma, P. Choudhary, P. Mittal, S. Kumar, A. Gouda and V. Krishnan, *ACS Catal.*, 2024, **14**, 4211–4248.
7 G. Pan, S. Cheng, Y. Zhang, Y. Chen, X. Xu and J. Xu, *Chem. Commun.*, 2023, **59**, 3301–3304.
8 P. Choudhary, A. Bahuguna, A. Kumar, S. S. Dhankhar, C. Nagaraja and V. Krishnan, *Green Chem.*, 2020, **22**, 5084–5095.
9 D. Sharma, P. Choudhary, S. Kumar and V. Krishnan, *J. Colloid Interface Sci.*, 2024, **657**, 449–462.
10 X. Zhang, B. Zhang and X. Li, *Org. Lett.*, 2021, **23**, 1687–1691.
11 D. Baidilov, D. Hayrapetyan and A. Y. Khalimon, *Tetrahedron*, 2021, **98**, 132435.
12 M. Pang, J.-Y. Chen, S. Zhang, R.-Z. Liao, C.-H. Tung and W. Wang, *Nat. Commun.*, 2020, **11**, 1249.
13 R. Lopes, Á. Raya-Barón, M. P. Robalo, C. Vinagreiro, S. Barroso, M. J. Romão, I. Fernández, M. M. Pereira and B. Royo, *Eur. J. Inorg. Chem.*, 2021, **2021**, 22–29.
14 T. G. Linford-Wood, N. T. Coles and R. L. Webster, *Green Chem.*, 2021, **23**, 2703–2709.
15 S. Kumar, P. Choudhary, D. Sharma, D. Sajwan, V. Kumar and V. Krishnan, *ChemSusChem*, 2024, e202400737.
16 R. Nie, Y. Tao, Y. Nie, T. Lu, J. Wang, Y. Zhang, X. Lu and C. C. Xu, *ACS Catal.*, 2021, **11**, 1071–1095.
17 B. Kashyap, S. Kumar, D. Sharma and V. Krishnan, *ChemNanoMat*, 2025, **11**(6), e202500117.
18 D. Sharma, P. Choudhary, S. Sheoran, S. Kumar, S. Bhattacharya and V. Krishnan, *Adv. Sustainable Syst.*, 2025, 2401006.
19 D. Sharma, D. Sajwan, S. Mishra, A. Gouda, P. Mittal, P. Choudhary, B. P. Mishra, S. Kumar and V. Krishnan, *Nanoscale Horiz.*, 2025, **10**(3), 423–459.
20 S. Kumar, D. Sajwan, D. Sharma and V. Krishnan, *Adv. Sustainable Syst.*, 2025, **9**, 2500003.
21 T. Wang, A. Hu, H. Wang and Y. Xia, *J. Chin. Chem. Soc.*, 2019, **66**, 1610–1618.
22 J. Feng, Y. He, Y. Liu, Y. Du and D. Li, *Chem. Soc. Rev.*, 2015, **44**, 5291–5319.
23 Z. Wang, Y. Chen, X. Li, G. He, J. Ma and H. He, *Environ. Sci. Technol.*, 2022, **56**, 1386–1394.
24 T. K. N. Nguyen, N. Dumait, F. Grasset, S. Cordier, D. Berthebaud, Y. Matsui, N. Ohashi and T. Uchikoshi, *ACS Appl. Mater. Interfaces*, 2020, **12**, 40495–40509.
25 S. Zhu, Y. Chen, M. A. Khan, H. Xu, F. Wang and M. Xia, *ACS Appl. Mater. Interfaces*, 2022, **14**, 7450–7463.
26 R. Ramachandran, Y. Lan, Z.-X. Xu and F. Wang, *ACS Appl. Energy Mater.*, 2020, **3**, 6633–6643.
27 L. Vigna, A. Nigro, A. Verna, I. V. Ferrari, S. L. Marasso, S. Bocchini, M. Fontana, A. Chiodoni, C. F. Pirri and M. Cocuzza, *ACS Omega*, 2021, **6**, 20205–20217.
28 M. Zhang, Y. Liu, B. Liu, Z. Chen, H. Xu and K. Yan, *ACS Catal.*, 2020, **10**, 5179–5189.
29 L. Jin, X. Zhou, F. Wang, X. Ning, Y. Wen, B. Song, C. Yang, D. Wu, X. Ke and L. Peng, *Nat. Commun.*, 2022, **13**, 6093.
30 I. Velázquez-Hernández, J. L. Lopez-Miranda, C. Ramos-Castillo, M. A. Gonzalez-Reyna, R. Esparza, N. Arjona and M. Estévez, *ACS Appl. Nano Mater.*, 2024, **7**, 22617–22630.
31 L. Jin, Y. Sun, X. Zhou, J. Wen, F. Wang, X. Ning, Y. Wen, D. Wu and L. Peng, *ACS Sustainable Chem. Eng.*, 2022, **10**, 12955–12961.
32 Q. Zhang, Y. Wang, J. Han, H. Liu, H. Zhang, Z. Wu, S. Zhang, W. Han and X. Ye, *Langmuir*, 2024, **40**(33), 17430–17443.
33 K. Parida and L. Mohapatra, *Chem. Eng. J.*, 2012, **179**, 131–139.
34 I. Palinko, P. Sipos, O. Berkesi and G. Varga, *J. Phys. Chem. C*, 2022, **126**, 15254–15262.
35 M. Shabanian, M. Hajibeygi and A. Raeisi, in *Layered Double Hydroxide Polymer Nanocomposite*, Elsevier, 2020, pp. 77–101.
36 C. Jing, Y. Chen, X. Zhang, X. Guo, X. Liu, B. Dong, F. Dong, X. Zhang, Y. Liu, S. Li and Y. Zhang, *Ind. Eng. Chem. Res.*, 2019, **58**, 11985–11998.
37 L. Feng, Y. Du, J. Huang, L. Cao, L. Feng, Y. Feng, Q. Liu, D. Yang and K. Kajiyoshi, *Sustainable Energy Fuels*, 2020, **4**, 2850–2858.
38 M. Li, J. E. Zhu, L. Zhang, X. Chen, H. Zhang, F. Zhang, S. Xu and D. G. Evans, *Nanoscale*, 2011, **3**, 4240–4246.
39 F. L. Theiss, G. A. Ayoko and R. L. Frost, *J. Therm. Anal. Calorim.*, 2013, **112**, 649–657.
40 E. Bernard, W. J. Zucha, B. Lothenbach and U. Mäder, *Cem. Concr. Res.*, 2022, **152**, 106674.
41 Z. Li, X. Chen, G. Huang, J. Wang, Y.-T. Sham, M. Pan and J. Bi, *Appl. Surf. Sci.*, 2024, **644**, 158728.
42 B. Ma, C. Zhang, D. Jia, Q. Zhao and P. Yang, *J. Phys. Chem. C*, 2023, **127**, 2908–2917.
43 H. Li, S. Li, R. Guan, Z. Jin, D. Xiao, Y. Guo and P. Li, *ACS Catal.*, 2024, 12042–12050, DOI: 10.1021/acscatal.4c03245.
44 X. Zhao, H. Li, M. Zhang, W. Pan, Z. Luo and X. Sun, *ACS Appl. Mater. Interfaces*, 2022, **14**, 34781–34792.
45 Y. Guan, J. Qin, X. Guo, Z. Li, H. Guo, M. Zhang, B. Zhang and J. Tang, *ACS Appl. Energy Mater.*, 2022, **5**, 12305–12314.
46 X. Chen, B. Fan, H. Wang, X. Liu, Y. Liu and J. Gao, *Inorg. Chem.*, 2024, **63**, 5132–5141.
47 M.-J. Zhou, T. Xu and J.-M. Hu, *Surf. Coat. Technol.*, 2021, **421**, 127416.
48 Q. Sun, L. Chang, Y. Liu, W. Nie, M. Lian and H. Cheng, *ACS Appl. Mater. Interfaces*, 2023, **15**, 43942–43952.
49 Z. Jiang, L. Yan, J. Wu, X. Liu, J. Zhang, Y. Zheng and Y. Pei, *Appl. Surf. Sci.*, 2020, **531**, 147281.

50 M. A. Al-Ghouti and D. A. Da'ana, *J. Hazard. Mater.*, 2020, **393**, 122383.
51 M. Li, H. Li, X. Jiang, M. Jiang, X. Zhan, G. Fu, J.-M. Lee and Y. Tang, *J. Mater. Chem. A*, 2021, **9**, 2999–3006.
52 K. Kumari and V. Krishnan, *ACS Sustainable Chem. Eng.*, 2025, **13**, 17740–17752.
53 H. Lv, H. Rao, Z. Liu, Z. Zhou, Y. Zhao, H. Wei and Z. Chen, *J. Energy Storage*, 2022, **52**, 104940.
54 J. Song, M. Hua, X. Huang, A. Visa, T. Wu, H. Fan, M. Hou, Z. Zhang and B. Han, *Green Chem.*, 2021, **23**, 1259–1265.
55 H. Liu, J. Zhao, Q. Li, X.-Y. Zhang, Z.-W. Zheng, K. Huang, D.-B. Qin and B. Zhao, *Chin. Chem. Lett.*, 2024, 110593.
56 R. Cohen, C. R. Graves, S. T. Nguyen, J. M. L. Martin and M. A. Ratner, *J. Am. Chem. Soc.*, 2004, **126**, 14796–14803.
57 E. D. Williams, K. A. Krieger and A. R. Day, *J. Am. Chem. Soc.*, 1953, **75**, 2404–2407.
58 Z. An and J. Li, *Green Chem.*, 2022, **24**, 1780–1808.
59 J. Blömer, D. Maga, J. Röttgen, Z. Wu, M. Hiebel, S. Eilebrecht, S. Jentsch and N. Eggers, *Chem. Ing. Tech.*, 2024, **96**, 561–574.
60 M. Shi, X. Zheng, N. Zhang, Y. Guo, M. Liu and L. Yin, *TrAC, Trends Anal. Chem.*, 2023, 117211.
61 A. P. Dicks and A. Hent, *Green Chem., metrics: a guide to determining and evaluating process greenness*, Springer, 2014.
62 T. Chhabra, A. Bahuguna, S. S. Dhankhar, C. Nagaraja and V. Krishnan, *Green Chem.*, 2019, **21**, 6012–6026.
63 T. Chhabra, P. Dwivedi and V. Krishnan, *Green Chem.*, 2022, **24**, 898–910.
64 C. R. McElroy, A. Constantinou, L. C. Jones, L. Summerton and J. H. Clark, *Green Chem.*, 2015, **17**, 3111–3121.
65 S. Kumar, P. Choudhary, D. Sharma and V. Krishnan, *ChemNanoMat*, 2025, **11**, e202400564.